RESEARCH

Experimental determination of Rayleigh scattering cross-sections at 408 nm

Yangzhuoran Liu[1] · Maria Dolores Andrés Hernández[1] · Midhun George[1,2] · John Philip Burrows[1]

Abstract

Cavity ring-down spectroscopy (CRDS) has been applied to retrieve accurate Rayleigh scattering cross-sections, $\sigma_{Rayl.}$ for a set of atmospheric gases at ~408 nm. Step pressure changes and pressure ramps were used in three different but similar optical cavities to measure light extinction by N_2, O_2, Ar, CO, CO_2, N_2O, CH_4 and synthetic air (SA). The experimentally determined $\sigma_{Rayl.}$ were compared with $\sigma_{Rayl.}$ values calculated for these atmospheric gases using knowledge of extrapolated literature values of the refractive index (n) and King correction factors measured in different spectral regions.

The difference between measured and calculated $\sigma_{Rayl.}$ using the most recently published dispersion relationship for N_2O and CH_4 is ~0.6%. This confirms the improved accuracy of the new dispersion relationship. The calculated and measured $\sigma_{Rayl.}$ agreed on average within 0.6%, 2.4%, 1.2%, 2.2%, and 1.5% for the gases CO_2, N_2 O_2, SA, and Ar at ~408 nm. However, for CO, the difference is 4.1%, i.e. more than twice the error. This implies that improved knowledge of the dispersion relationship for CO, and thus the refractive index and King correction factors, would be of value to calculate $\sigma_{Rayl.}$ in the blue spectral region.

1 Introduction

A sufficiently accurate knowledge of the Rayleigh scattering cross-section, $\sigma_{Rayl.}(\widetilde{\nu})$, of gases and of the complex refractive index of particles [1] over large wavenumber ($\widetilde{\nu}$) or wavelength (λ) ranges enables to understand the scattering of electromagnetic radiation and is an essential prerequisite for many applications. For example, $\sigma_{Rayl.}(\widetilde{\nu})$ are required for the remote sensing of trace gases aerosol and cloud parameters (e.g. [2, 3]), the atmospheric radiative transfer modelling of the Earth and other planetary atmospheres and for the estimation of the extinction properties of clouds and aerosols in studies of climate change [4–6].

In the past decades, optical techniques, such as cavity ring-down spectroscopy (CRDS) [7] and broadband cavity enhanced spectroscopy (BBCES) [8, 9], have been used

✉ Yangzhuoran Liu
  lyzr@iup.physik.uni-bremen.de

✉ Maria Dolores Andrés Hernández
  lola@iup.physik.uni-bremen.de

1 Institute of Environmental Physics, University of Bremen, Bremen, Germany

2 Currently at School of Chemistry, University of Leeds, Leeds, UK

to determine accurate values of the $\sigma_{Rayl.}(\widetilde{\nu})$ for a variety of atmospheric molecules (e.g. [1, 10–12]). The value for $\sigma_{Rayl.}(\widetilde{\nu})$ at $\widetilde{\nu}$ [cm^{-1}] for a gas of number density N [molec. $\cdot$ cm^{-3}] [13, 14] depends on the refractive index $n_{\widetilde{\nu}}$ and the King correction factors $F_k(\widetilde{\nu})$ for non-spherical molecules [15]. The $\sigma_{Rayl.}(\widetilde{\nu})$ are calculated using Eq. (1):

$$\sigma_{Rayl}(\widetilde{\nu}) = \frac{24\pi^3\widetilde{\nu}^4}{N^2}\left(\frac{n_{\widetilde{\nu}}^2 - 1}{n_{\widetilde{\nu}}^2 + 2}\right)^2 F_k(\widetilde{\nu}) \tag{1}$$

If there are no measured values of $n_{\widetilde{\nu}}$ and $F_k(\widetilde{\nu})$ at a selected $\widetilde{\nu}$, they are estimated by extrapolating the fits of $n_{\widetilde{\nu}}$ and $F_k(\widetilde{\nu})$ in a given range of $\widetilde{\nu}$ to the selected $\widetilde{\nu}$. Equation (1) is then used to estimate $\sigma_{Rayl.}(\widetilde{\nu})$. However, the $\widetilde{\nu}$ dependency of $n_{\widetilde{\nu}}$ and $F_k(\widetilde{\nu})$, lead to $\sigma_{Rayl.}(\widetilde{\nu})$ not being exactly proportional to $\widetilde{\nu}^4$. Consequently, $\sigma_{Rayl.}(\widetilde{\nu})$, at a selected $\widetilde{\nu}$, calculated using Eq. (1) and values of $n_{\widetilde{\nu}}$ and $F_k(\widetilde{\nu})$ extrapolated from dispersion relationships in another $\widetilde{\nu}$ range may be inaccurate and have to be used with caution [11, 16]. Of relevance to this study, there are only a limited number of experimentally determined $\sigma_{Rayl.}(\widetilde{\nu})$ values in the near UV and blue spectral region [17–20]. The comparison of measured and calculated $\sigma_{Rayl.}(\widetilde{\nu})$. enables the accuracy of the extrapolated $n_{\widetilde{\nu}}$ and $F_k(\widetilde{\nu})$ to be assessed.

Recently, BBCES has been established as an effective way of measuring the optical extinction of gases and aerosols. The technique has high sensitivity and good reproducibility [1, 16–21]. The use of broadband optical sources, coupled with spectrally resolving spectrometers and multichannel detectors, enables the scattering properties of molecules over broad spectral regions to be investigated. However, the accuracy of the BBCES measurements of extinction depends on the knowledge of the mirror reflectivity across the broadband spectral range investigated. This is estimated from the difference between the extinction measured with the cavity filled with molecular nitrogen (N_2) or with Helium (He) [12, 16].

In contrast to BBCES, the CRDS technique is considered an absolute method. In CRDS, measurements of the rate of decay of the laser radiation in the cavity or optical resonator, after a laser is switched off, yield the so-called cavity ring-down times τ. The latter depends on the density of molecules present in the cavity, which absorb or scatter. In the absence of absorption by a gas, the measurement of the extinction of radiation by CRDS yields an accurate experimental verification of the $\sigma_{Rayl.}(\widetilde{\nu})$ for gases at the laser $\widetilde{\nu}$. For this reason, spectral regions having no absorption by a target gas are selected for the determination of $\sigma_{Rayl.}(\widetilde{\nu})$. Any additional losses of radiation (e.g. because of absorption by the cavity mirrors) are constant as a function of pressure and can be accounted for in the analysis. In the following, $\sigma_{Rayl.}(\widetilde{\nu})$ is calculated using Eq. (1) where the value of $\widetilde{\nu}$ is estimated from the measurements of the laser wavelength, λ. Consequently, λ rather than $\widetilde{\nu}$ will be hereafter used in the text, e.g. $\sigma_{Rayl.}(\lambda)$.

The extinction coefficient $\alpha(\lambda)$ in an optical cavity is defined as:

$$\alpha(\lambda) = N \times \sigma(\lambda) = \frac{n(\lambda)}{c_0} \times \left(\frac{1}{\tau(\lambda)} - \frac{1}{\tau_0(\lambda)} \right) \qquad (2)$$

where N is the gas number density [molec. $\cdot$ cm^{-3}], λ is the wavelength, $\sigma(\lambda)$ is the extinction cross-section [cm$^2 \cdot$ molec.$^{-1}$] at the measured wavelength λ, $n(\lambda)$ is the refractive index of the molecule, c_0 is the speed of light in vacuum, $\tau(\lambda)$ and $\tau_0(\lambda)$ are the cavity ring-down times of the filled and the empty cavity, respectively. In the absence of absorption, it is assumed that $\sigma(\lambda) = \sigma_{Rayl.}(\lambda)$.

In the last decade, CRDS has been used to retrieve the $\sigma_{Rayl.}(\lambda)$ for different molecules at a discrete number of wavelengths in the UV and UV–Vis spectral regions. Some examples of such studies are for the following gases: argon (Ar), N_2 and sulphur hexafluoride (SF_6) in the region 560 – 650 nm [10]; N_2, and Ar in the region 470 – 490 nm; carbon monoxide (CO), carbon dioxide (CO_2), nitrous oxide (N_2O), methane (CH_4) and SF_6 in the region 467 – 574 nm [11]; N_2, CH_4 and SF_6 up to 270 nm [22]; N_2 at 405.8 and

532.2 nm [17, 18]; He, CO_2, N_2O, SF_6, oxygen, O_2, CH_4 at 404 and 662 nm) [20].

In a previous paper, George et al. [23] described the development of CRDS detectors as part of an instrument which determined the ambient concentrations of peroxy radicals after their conversion to nitrogen dioxide (NO_2) by chemical amplification. There are few measured values of $\sigma_{Rayl.}(\lambda)$ at 408 nm or close by and the availability of these characterised cavities, thus, provided an opportunity to measure accurately $\sigma_{Rayl.}(\lambda)$ for different gases using three different diode lasers emitting blue radiation. In the present study, the $\sigma_{Rayl.}(\lambda)$ of the atmospheric relevant N_2, O_2, Ar, CO, CO_2, N_2O and CH_4 have been derived from CRDS measurements at 408 nm. N_2 and O_2 are the most abundant gases in the atmosphere. In the absence of clouds, molecular scattering dominates the atmospheric extinction of solar radiation and precise values of the $\sigma_{Rayl.}(\lambda)$ of N_2, O_2 and CO_2 are, therefore, of particular importance for the retrieval of atmospheric profiles of aerosol and clouds [24]. In addition, N_2 is used for several optical applications in atmospheric studies [9, 25, 26]. CO_2, N_2O and CH_4 are important greenhouse gases and as for the case of CO, measurements of their refraction indices and King correction factors in the UV–Vis range are scarce. At this wavelength, the molecules investigated do not have significant structured absorption features and the light extinction is expected to be dominated by Rayleigh scattering.

2 Experimental

Figure 1 shows schematically the CRDS measurement setup used for the determination of $\sigma_{Rayl.}$ at $\lambda \sim 408$ nm of the bulk and trace atmospheric gases investigated: N_2, O_2, SA, Ar, CO, CO_2, N_2O and CH_4. The SA used in this study contains ≤ 2.1 mol ppm Ar (For further gas specifications, see Table S.3 in the supplement).

The experimental setup comprises a continuous wave multimode diode laser with a power output of 100 mW (Stradus 405, $\cong 408$ nm, 100 mW max output power, Vortran Laser Technology Inc.), aligned to an optical V-shape cavity with three highly reflective mirrors (reflectivity, $R = 99.995\%$; diameter, $d = 0.5''$; AT Films, USA). The electromagnetic radiation transmitted through the end mirrors of the cavity is directed to the Si photodiode detector and to a beam camera (BM-USB-SP907-OSI, Ophir Spiricon Europe GmbH) to monitor the cavity output and the laser mode shape, respectively. Three different setups, comprising a cavity, diode laser and Si photodiode, were used to measure the ring-down times which were then used to determine the $\sigma_{Rayl.}$ of the different gases. In the following, they are called setup 1, setup 2 and setup 3. They differ in the radius of curvature of the front mirror of the V-shape cavity,
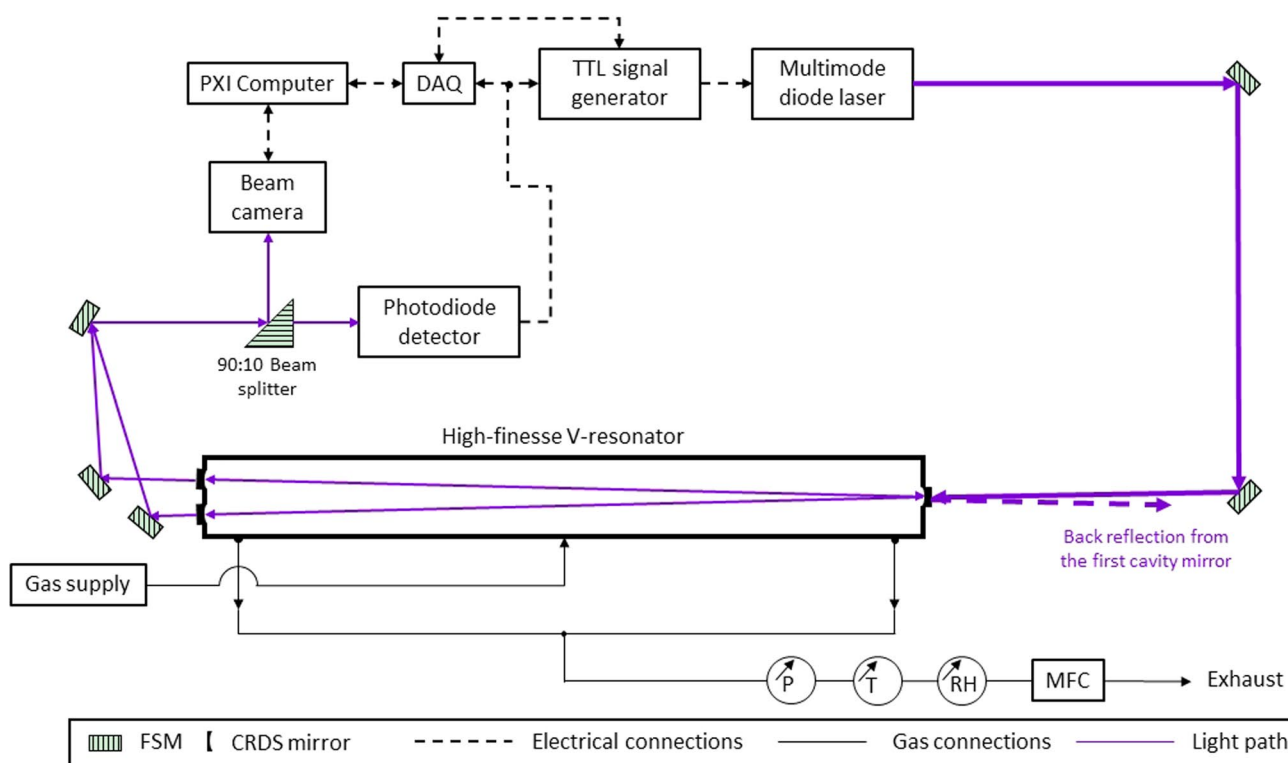
Fig. 1 Schematic diagram of CRDS setup used for the $\sigma_{Rayl.}$ determination in this study. PXI: PCI extensions for instrumentation, DAQ: data acquisition system, TTL: transistor to transistor logic, FSM: front silvered aluminium mirror, P: pressure sensor, T: temperature sensor, RH: relative humidity sensor, MFC: mass flow controller

roc, (roc = 100 cm for setups 1 and 2, and roc = 200 cm for setup 3) and the Si photodiode (type HCA-S, spectral range 300–1000 nm, active diameter 0.8 mm, bandwidth 2 MHz, gain 1 MV/A, Femto Messtechnik GmbH for setups 1 and 2, and type OE-200-SI, Femto Messtechnik GmbH spectral range 320–1060 nm, active diameter 1.2 mm, bandwidth 0.4 MHz, gain 5 MV/A for setup 3). The V-shaped cavities used have lengths of 39 cm for setups 1 and 2 and 32 cm for setup 3. Consequently, the free spectral range of these cavities is much smaller than that of the laser diode. Therefore, it is expected that all the longitudinal modes from the laser can couple to the CRDS cavity. During the detector operation, 10^6 samples $\cdot$ s^{-1} signal of the photodiode are averaged and fitted using a Levenberg Marquardt algorithm to a single exponential decay, which is then recorded at a 1 Hz frequency ring-down time (for a more detailed description, see [23]).

In these experiments, the cavity is filled with the gas of interest. Each setup has two different modes of operation. The pressure is changed in the range from 300 to 700 hPa either a) in pressure steps using continuous gas flows, this is called the continuous mode of operation, or b) by increasing the pressure from 300 to 1300 hPa, i.e. having pressure ramps, which is known as the ramp mode. The pressure is continuously monitored using two sensors (Sensor Technics:

HCX001A6V-1714 for setup 1 and setup 2, and MKS: 626AX13TQE for setup 3). The measurement of pressure in the setups had $\pm 1\%$ accuracy and linearity in the range 100–1000 mbar. This was determined by calibration using an absolute pressure sensor (Greisinger GDH 12AN). In addition, the humidity (Honeywell: HIH-4000–1311 for setup 1 and setup 2, and Vaisala: HMP238 for setup 3) and the temperature (Analog Devices: AS22100, which has a ± 1 °C accuracy for setup 1 and setup 2, and Vaisala HMP238, which has a ± 0.1 °C accuracy, for setup 3) in the cavity are continuously measured.

In the continuous mode of operation, the gas enters the cavity from both ends and leaves the cavity from the middle exit at a constant rate. The latter is changed in steps of 5 or 10 min duration by a mass flow controller, which is connected to a vacuum pump. In the pressure ramp mode, the cavity is flushed with the gas of interest at a flow rate of 1000 cm^3 $\cdot$ min^{-1} at 300 hPa until the ring-down time and the relative humidity are stable. The exit line is then closed until the standard deviation (1σ) of the τ signal remains < 0.007 µs per h. The pressure ramp is then initiated by gas addition using a flow of 20 cm^3 $\cdot$ min^{-1}. This leads to gas accumulation, i.e. to a continuous pressure increase in the cavity up to ~ 1300 hPa. Similarly, short inverse pressure ramps were occasionally carried out by a subsequent gas release at a

	a	b	μ (nm)	σ (nm)	FWHM (nm)	$\sum \chi^2$
a)	0.66	0.02	407.9	0.57	1.33	0.03
b)	0.64	0.01	408.3	0.64	1.41	0.02
c)	0.87	0.00	408.4	0.44	1.04	0.01
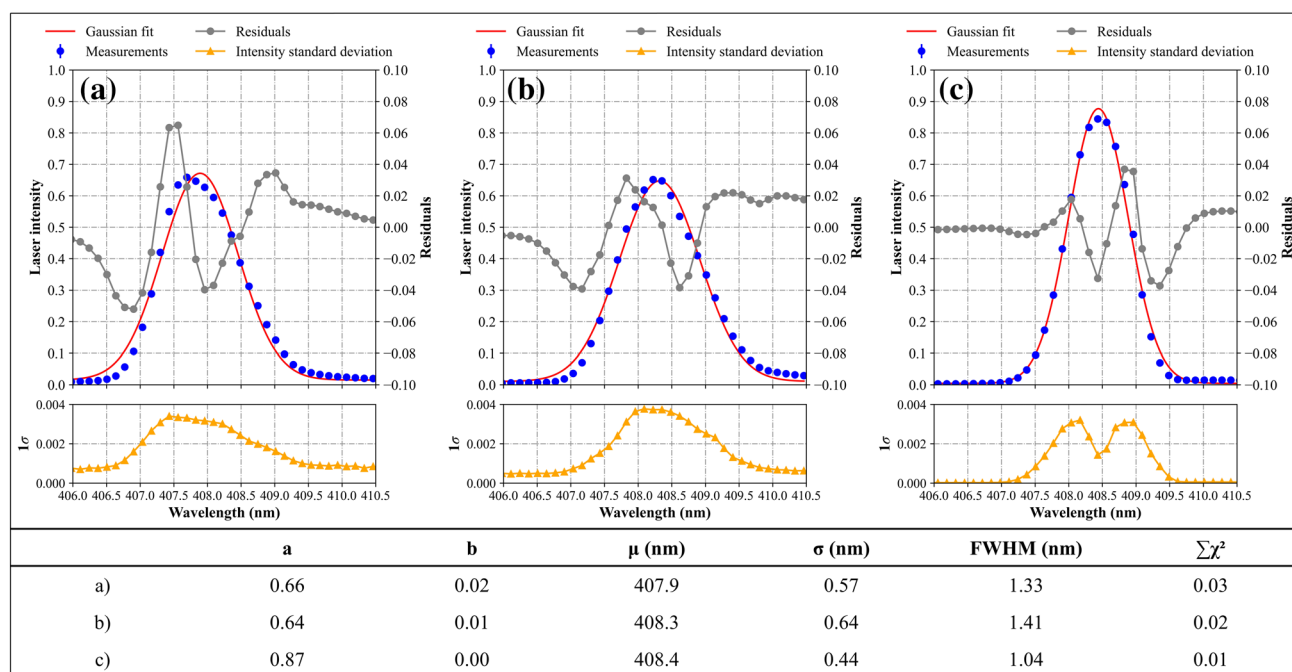
Fig. 2 Examples of the determination of the wavelength of the maximum intensity for the lasers used in this study: (a) setup 1, (b) setup 2, (c) setup 3. The counts at each wavelength λ are normalised to the total intensity measured during 60 min (blue measurement points). The parameters of the Gaussian fit applied (red line), i.e. **a**: height of the curve, **b**: offset of the curve, **μ**: centre of the peak, **σ**: Gaussian root mean square width, **FWHM**: full-width half maximum and **χ**: difference between fitted and measured values. The residual of the fit is shown in grey and the 1σ standard deviation of the normalised intensity is shown in yellow

rate of $20 \, \text{cm}^3 \cdot \text{min}^{-1}$ to ambient pressures. To minimise the time required for cavity stabilisation by gases such as CO, O_2, N_2O and N_2, the filled cavity was left closed at 300 hPa the night before the ramp experiment. For these experiments, it is essential that the cavity is leak tight to prevent room air leaks into the cavity, which would then scatter and thereby interfere with the measurements made during the pressure ramps. The setup 3 used for the ramp experiments had the lowest rates of pressure leak ($\leq 0.01 \, \text{hPa} \cdot \text{min}^{-1}$). From the measured increase in pressure observed, the interference caused by the diffusion of the ambient air into the cavity is estimated to be $< 1\%$.

The spectral output and maximum intensity of the multimode lasers in the experiments were determined using a spectrometer (Avantes AvaSpec-ULs2048 × 64 ENV11, SN: 1803001U1. 295 nm—535 nm grating, 200 μm slit, 0.74 ± 0.04 nm resolution (FWHM), 1200 lines/mm), previously calibrated with a Hg (Ar) emission pen-ray lamp. A Gaussian fit of the signal counts normalised to the total intensity was applied, using 60 min averages of the 1 Hz sample rate from 406 to 410.5 nm. Figure 2 shows the peak wavelength values (μ) determined for the lasers used in this study, which operated with a power of 100 mW. The shape of the laser emission line was stable within 98.5% of the normalised intensity during the 60 min measurements. In addition, supporting measurements

were taken by a wavelength metre (Bristol 621, SN: 6081; 350 nm $< \lambda <$ 1100 nm, accuracy: ± 0.2 ppm aka. ± 0.0001 nm @ 500 nm). The back-reflected beam from the first cavity mirror was directed to the wavelength metre, whereas the spectrometer detected one of the outgoing beams from the V-shaped cavity. The 1 h measurements were repeated up to the maximum input power supported by the wavemeter. The wavelength of the laser measured by the wavelength metre and the spectrometer agreed within the experimental error of the two measurements, i.e. $\pm 0.09 - 0.16$ nm (2σ) for the wavelength metre and λ peak $\pm 0.36 - 0.44$ nm (HWHM) for the spectrometer.

Equation. (1) is used to calculate the n-based $\sigma_{\text{Rayl.}}(\lambda)$ for each molecule under investigation. This involves the convolution of the high-resolution literature n-based $\sigma_{\text{Rayl.}}(\lambda)$ with the spectral output around the peak wavelength μ (nm) measured for each laser by the spectrometer and assuming a Gaussian FWHM. Table S.2 in the supplement provides more details about the used refractive indices, King correction factors and references for the calculation of each molecule.

The use of three different setups enables the investigation of any impact on the values of $\sigma_{\text{Rayl.}}$ at $\lambda \sim 408$ nm arising from differences in laser wavelengths, which are

small, mirror reflectivities, cavity tightness and modes of operation.

3 Results and discussion

In Fig. 3, an example of the $\sigma_{Rayl.}(\lambda)$ determination from the CRDS measurements is shown for O_2. A linear fit is applied to the loss rate $1/(\tau c)$ [cm^{-1}] and N of the molecule of interest [molec. · cm^{-3}], Eq. (3), shown below, is obtained by rearranging Eq. (2):

$$\frac{1}{\tau(\lambda)c} = N \times \sigma_{(\lambda)} + \frac{1}{\tau_0(\lambda)c} \tag{3}$$

where c is the speed of the electromagnetic radiation in the gas investigated, i.e. O_2 and $c = c_0/n(\lambda)$. $n(\lambda)$ is not determined experimentally in this study but calculated using the dispersion relationship measured at different wavelengths and interpolated or extrapolated to the λ of the laser used in the experiment. The slope or gradient, i.e. $\sigma_{(\lambda)}$ of the fit is the Rayleigh scattering cross-section [cm^2 · molec.$^{-1}$]. The y intercept at $N = 0$ is related to the τ_0 of the cavity, i.e. $y = 1/(\tau_0 c)$.

Table 1 summarises the experimental values of $\sigma_{Rayl.}(\lambda)$ and an error or uncertainty of two standard deviations (2σ) for the measurements of different gases using the method described above. For the molecules investigated, the noise is $< 0.2\%$ of the CRDS signal as indicated in Table S.1 in the supplement. The $\sigma_{Rayl.}(\lambda)$ values obtained using different measurement modes (i.e. continuous and ramp) at the same λ agree within the experimental error, as shown for the values of $\sigma_{Rayl.}(\lambda)$ determined using the setup 3.
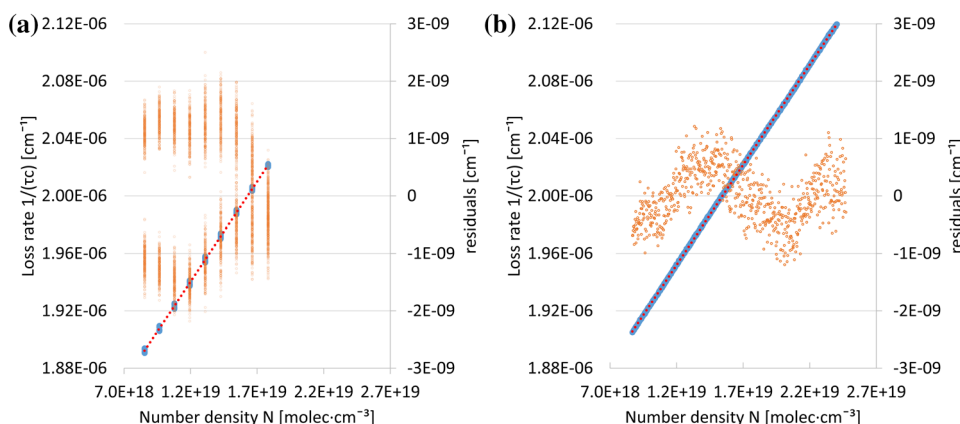
Fig. 3 Example of CRDS measurement for the σRayl determination of O_2 at 408.4 nm using setup 3, (**a**) continuous mode, 90 min measurement duration, 4115 signal points; (**b**) ramp mode, 11 min measurement duration, 695 signal points. The measurements are shown as blue dots, the fitting as red dashed lines, the orange circles are the residuals which correspond with the measured loss rate minus the loss rate of the fit. The determined $\sigma_{Rayl.}$ for O_2 are the slopes of the fitting lines

Table 1 Rayleigh scattering cross-sections determined by CRDS in this study

$\sigma_{Rayl.}$/Gas		N$_2$	O$_2$	SA	Ar	CO	CO$_2$	N$_2$O	CH$_4$
Setup 1 (407.9 nm) continuous	Mean ($\times 10^{-26}$ cm^2)	1.562	1.377	1.501	1.348	n.a	n.a	n.a	3.403
	2σ ($\times 10^{-26}$ cm^2)	0.018	0.012	0.005	0.027	n.a	n.a	n.a	0.021
	Number of measurements	16	2	11	11	n.a	n.a	n.a	4
Setup 2 (408.3 nm) continuous	Mean ($\times 10^{-26}$ cm^2)	1.552	1.374	1.495	1.337	n.a	n.a	5.428	n.a
	2σ ($\times 10^{-26}$ cm^2)	0.003	0.008	0.009	0.016	n.a	n.a	0.035	n.a
	Number of measurements	5	7	14	9	n.a	n.a	15	n.a
Setup 3 (408.4 nm) continuous	Mean ($\times 10^{-26}$ cm^2)	1.521	1.391	1.502	1.324	1.938	3.989	5.478	3.447
	2σ ($\times 10^{-26}$ cm^2)	0.016	0.006	0.018	0.029	0.011	0.019	0.010	0.018
	Number of measurements	14	23	7	48	14	26	13	19
Setup 3 (408.4 nm) ramp	Mean ($\times 10^{-26}$ cm^2)	1.515	1.393	1.524	1.327	1.953	3.975	5.485	3.450
	2σ ($\times 10^{-26}$ cm^2)	0.014	0.004	0.014	0.033	0.021	0.064	0.008	0.050
	Number of measurements	11	6	11	13	6	7	4	9

Mean values and 2σ errors are indicated. *n.a.* not available. CO is a toxic and explosive gas. For safety reasons, the CO measurements were only made with the setup 3
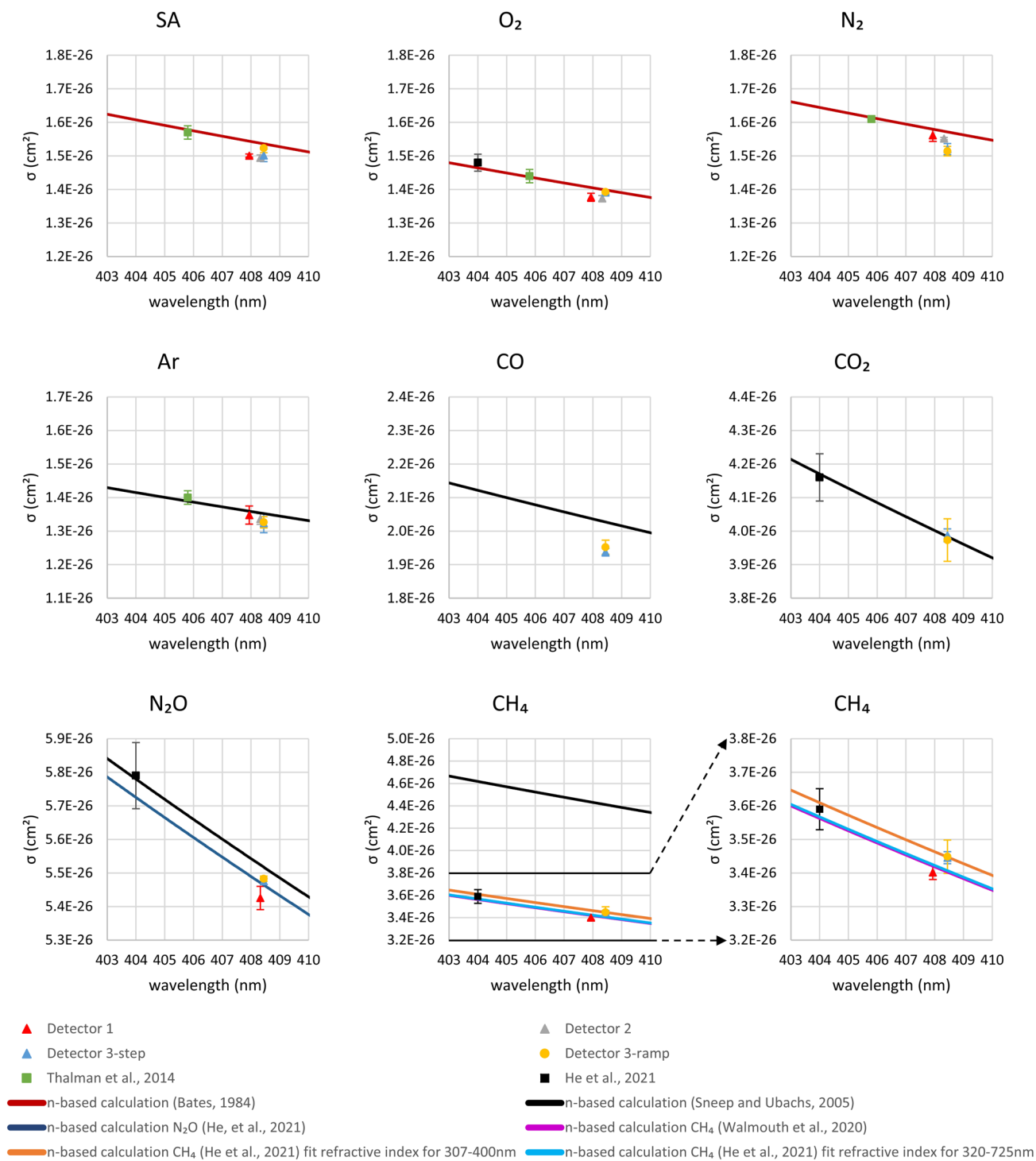
Fig. 4 Rayleigh scattering cross-sections $\sigma_{\mathrm{Rayl.}}(\lambda)$ for N_2, O_2, Ar, CO, CO_2, N_2O and CH_4 available in the literature in the range $403 \leq \lambda \leq 410$ nm and the measurements made in this study. The $\sigma_{\mathrm{Rayl.}}(\lambda)$ experimentally obtained in this study are shown as follows: triangles for continuous measurements (red, grey and blue for setup 1, 2 and 3, respectively) and yellow dots for the ramp measurements. Previous CRDS measurements: from Thalman et al. [17] and He et al. [20] are also indicated in squares (green and black, respectively). The continuous lines show the calculations of $\sigma_{\mathrm{Rayl.}}(\lambda)$ using Eq. (1) from Bates, (in dark red) [27], Sneep and Ubachs (in black) [11], He et al. N_2O (dark blue) [20], He et al. CH_4 with fitted refractive index based on measurement for 307—400 nm (in orange), 320—725 nm (in cyan) [20] and Wilmouth et al.(in magenta) [16]

Table 2 Calculated n-based $\sigma_{Rayl.}(\lambda)$ for the lasers used in the present study (see the refractive index, King correction factors and references in Table S.2 in the supplement)

n-based $\sigma_{Rayl.}$ ($\times 10^{-26}$ cm²)/Gas	N₂	O₂	SA	Ar	CO	CO₂	N₂O	CH₄
Setup 1 (407.9 nm)	1.580	1.406	1.544	1.358	2.037	4.008	5.493	3.465
Setup 2 (408.3 nm)	1.574	1.400	1.538	1.353	2.030	3.993	5.471	3.452
Setup 3 (408.4 nm)	1.572	1.399	1.536	1.351	2.027	3.988	5.464	3.448

During the CRDS measurements of N_2 and Ar in the continuous gas mode, the τ_0 of the cavities decreased by up to 15% and 18%, respectively. This gradual τ_0 and τ decrease along the series of measurements recover to their initial values after cleaning the mirrors. There is no obvious explanation for this effect. Nevertheless, it might be associated with either the deposition of an unknown impurity or impurities in the gases on the mirrors. Alternatively, a gradual gas saturation of the CRDS mirror surface in the coated layer of N_2 or Ar may explain this reproducible effect. Interestingly, this decrease is not observed in the measurements performed for SA over 10 months. In this period, the τ_0 change was < 3%. However, the small value of the standard deviation of the measured $\sigma_{Rayl.}(\lambda)$ of N_2 and Ar implies that the steady decrease of the decay time τ during the measurement does not significantly affect the $\sigma_{Rayl.}(\lambda)$ retrieved.

Differences in the values of $\sigma_{Rayl.}(\lambda)$ determined with different setups are partly explained by small differences in the wavelength of the individual laser setups used. The corresponding n-based $\sigma_{Rayl.}(\lambda)$, which are calculated as explained in the previous section using Eq. (1), are provided in Table 2.

In Fig. 4, the $\sigma_{Rayl.}(\lambda)$ which are available for the molecules investigated in the spectral range $403 \leq \lambda \leq 410$ nm are plotted as a function of λ. The values provided in the present study are consistent with previous measurements for O_2, Ar and CO_2 and SA. The obtained $\sigma_{Rayl.}(\lambda)$ agree on average within 0.6% with the calculated n-based $\sigma_{Rayl.}(\lambda)$ for CO_2, N_2O and CH_4, and within 2.4%, 1.2%, 2.2%, 1.5% and 4.1% for N_2, O_2, SA, Ar and CO, respectively. For CH_4 and N_2O, the retrieved $\sigma_{Rayl.}(\lambda)$ values provide independent experimental evidence, and thus confirm the revised values of $n(\lambda)$ reported by Wilmouth et al. [16] and He et al. [20] as part of their CRDS and BBCES studies of the $\sigma_{Rayl.}(\lambda)$ for these greenhouse gases in this wavelength range. He et al. [20] reported CH_4 absorption cross-sections $\approx 1 \times 10^{-27}$ cm² around 408 nm. This would imply a $\approx 3\%$ contribution of the absorption in the total extinction measured to retrieve the Rayleigh cross-sections in this study. For the case of N_2, the commonly accepted n-based $\sigma_{Rayl.}(\lambda)$ [11, 27] overestimate the experimental $\sigma_{Rayl.}$ at ≈ 408 nm. This overestimation of $\sigma_{Rayl.}(\lambda)$ of N_2 requires further investigation in other λ ranges.

4 Summary and conclusion

This study presents a consistent set of $\sigma_{Rayl.}(\lambda)$ experimentally determined by extinction measurements made by CRDS at ≈ 408 nm. The results obtained by continuous and pressure ramp measurement modes agree within their experimental error and the differences in the laser wavelength of the three configurations used to retrieve the $\sigma_{Rayl.}(\lambda)$. The reason for a gradual decrease observed in the τ_0 of the optical cavities during the N_2 and Ar measurement periods is not known but it does not affect the $\sigma_{Rayl.}(\lambda)$ retrieved. The $\sigma_{Rayl.}(\lambda)$ data obtained are consistent with previous literature measurements and calculations. The comparison with n-based $\sigma_{Rayl.}(\lambda)$ is in agreement within 0.6% for CO_2, N_2O and CH_4 and within 2.4%, 1.2%, 2.2%, 1.5% and 4.1% for N_2, O_2, SA, Ar and CO, respectively. This study provides for the first time experimentally retrieved CO $\sigma_{Rayl.}$ at 408 nm, which are significantly overestimated compared to the n-based $\sigma_{Rayl.}(\lambda)$ in this spectral range.

The retrieved $\sigma_{Rayl.}$ for the molecules investigated at 408 nm provide independent experimental evidence about the accuracy of dispersion relations used to estimate the $n(\lambda)$ and $F_k(\lambda)$ on the basis of single experiments. From the above, the dispersion relations for N_2 and CO need to be reinvestigated in the wavelength region around 408 nm.

Author contributions YL, MDAH and MG designed the experiments. YL carried out the measurements with the help from MG. MDAH and YL prepared the draft manuscript. JPB revised the manuscript. All authors agreed with the manuscript.

Data availability Data underlying the results presented in this paper are available upon request to the corresponding author.

Declarations

Conflict of interest The authors declare no conflicts of interest.

References

1. R.A. Washenfelder, J.M. Flores, C.A. Brock, S.S. Brown, Y. Rudich, Atmos. Meas. Tech. **6**, 861 (2013)
2. J.P. Burrows, M. Weber, M. Buchwitz, V. Rozanov, A. Ladstätter-Weißenmayer, A. Richter, R. DeBeek, R. Hoogen, K. Bramstedt, K.-U. Eichmann, M. Eisinger, D. Perner, J. Atmos. Sci. **56**, 151 (1999)
3. H. Bovensmann, J.P. Burrows, M. Buchwitz, J. Frerick, S. Noël, V.V. Rozanov, K.V. Chance, A.P.H. Goede, J. Atmos. Sci. **56**, 127 (1999)
4. V.V. Rozanov, D. Diebel, R.J.D. Spurr, J.P. Burrows, J. Geophys. Res. **102**, 16683 (1997)
5. V.V. Rozanov, M. Buchwitz, K.-U. Eichmann, R. de Beek, J.P. Burrows, Adv. Space Res. **29**, 1831 (2002)
6. A. Rozanov, V. Rozanov, M. Buchwitz, A. Kokhanovsky, J.P. Burrows, Adv. Space Res. **36**, 1015 (2005)
7. G. Berden, R. Peeters, G. Meijer, Int. Rev. Phys. Chem. **19**, 565 (2000)
8. S.E. Fiedler, A. Hese, A.A. Ruth, Chem. Phys. Lett. **371**, 284 (2003)
9. W. Chen, D.S. Venables, 3 - Broadband optical cavity methods, in: *Chen, Venables et al. (Ed.) 2021 – Advances in spectroscopic monitoring* .
10. H. Naus, W. Ubachs, Opt. Lett. **25**, 347 (2000)
11. M. Sneep, W. Ubachs, J. Quant. Spectrosc. Radiat. Transfer **92**, 293 (2005)
12. N. Jordan, C.Z. Ye, S. Ghosh, R.A. Washenfelder, S.S. Brown, H.D. Osthoff, Atmos. Meas. Tech. **12**, 1277 (2019)
13. R.J. Strutt, Proc. R. Soc. Lond. A **95**, 155 (1918)
14. L. Rayleigh, Proc. R. Soc. Lond. A **97**, 435 (1920)
15. L.V. King, Proc. R. Soc. Lond. A **104**, 333 (1923)
16. D.M. Wilmouth, D.S. Sayres, J. Quant. Spectrosc. Radiat. Transfer **255**, 107224 (2020)
17. R. Thalman, K.J. Zarzana, M.A. Tolbert, R. Volkamer, J. Quant. Spectrosc. Radiat. Transfer **147**, 171 (2014)
18. R. Thalman, K.J. Zarzana, M.A. Tolbert, R. Volkamer, J. Quant. Spectrosc. Radiat. Transfer **189**, 281 (2017)
19. D.M. Wilmouth, D.S. Sayres, J. Quant. Spectrosc. Radiat. Transfer **234**, 32 (2019)
20. Q. He, Z. Fang, O. Shoshanim, S.S. Brown, Y. Rudich, Atmos. Chem. Phys. **21**, 14927 (2021)
21. Q. He, N. Bluvshtein, L. Segev, D. Meidan, J.M. Flores, S.S. Brown, W. Brune, Y. Rudich, Environ. Sci. Technol. **52**, 3456 (2018)
22. D. Ityaksov, H. Linnartz, W. Ubachs, Mol. Phys. **106**, 2471 (2008)
23. M. George, M.D. Andrés Hernández, V. Nenakhov, Y. Liu, J.P. Burrows, Atmos. Meas. Tech **13**, 2577 (2020)
24. H. Horvath, Atmos. Environ. A. Gen. Top. **27**, 293 (1993)
25. J.M. Langridge, S.M. Ball, A.J.L. Shillings, R.L. Jones, Rev. Sci. Instrum. **79**, 123110 (2008)
26. S. John, M. Wang, J. Chen, A. Pakkatil, Y. Du, J. Zhang, A. Ramachandran, A. Saseendran, A.P. Thomas, D. Viswanathan, C. Mazzoleni, R. Varma, Aerosol Sci. Technol. **55**, 1264 (2021)
27. D.R. Bates, Planet. Space Sci. **32**, 785 (1984)